Rather et al

Research Article format

Key words (3-6): Mitochondria, nucleus, programmed cell death, phagocytosis

Summary Statement (29/30 words): This work describes the genetic control and cellular dynamics of a factor linked to cancer, metabolic and degenerative disease acting in developmentally dying cells to instruct their own removal.

Running title (31/32 characters): WAH-1/AIF phagocytic dynamics

Working title (108/120 characters):

EOR-1/PLZF-regulated WAH-1/AIF sequentially promotes early and late stages of non-apoptotic corpse removal

Nathan Rather[1], Melvin Williams[2], Aladin Elkhalil[1], Karen Juanez[1], Rashna Sharmin[1], Ginger Clark[1], Shai Shaham[2], Piya Ghose[1*]

[1]The University of Texas at Arlington

[2]The Rockefeller University

*To whom correspondence should be addressed.

piya.ghose@uta.edu

Abstract (159/180 words)

Programmed cell death (PCD) is a crucial genetically-encoded and evolutionarily-conserved process for development and homeostasis. We previously identified a genetically non-apoptotic, highly ordered, and stereotyped killing program called Compartmentalized Cell Elimination (CCE) in the *C. elegans* tail-spike epithelial cell (TSC). Here we identify the transcription factor EOR-1/PLZF as promoting CCE. Loss of EOR-1 results in a persisting un-engulfed large soma with enlarged nuclei. We find that EOR-1 and its partners positively regulate the transcription of the Apoptosis Inducing Factor AIF homolog, WAH-1/AIF. We report stereotyped and sequential spatiotemporal dynamics of WAH-1/AIF1 during phagocytosis, with

defined roles early and late. Mitochondrial to plasma membrane translocation is required for internalization, and plasma membrane to nuclear translocation for DNA degradation and ultimate corpse resolution. Our study expands our knowledge of PCD by describing a mechanistic contribution of EOR-1/PLZF and functional relevance to specific spatiotemporal contexts for WAH-1/AIF function, and by implying a correlation between DNA degradation with nuclear morphology during cell elimination.

Introduction

Programmed cell death (PCD) is a genetically programmed and evolutionarily conserved form of cell elimination vital for normal development and homeostasis (1). Defects can pose devastating consequences such as aberrant brain development and cancer therapy resistance(2-4). Apoptosis, arguably the most well studied form of PCD, is characterized by certain morphologic and genetic characteristics. Morphologically, apoptosis progresses by cell shrinkage, chromatin condensation, nuclear fragmentation, and mitochondrial fragmentation (1, 5, 6). Genetically, apoptosis is controlled by several conserved regulators including the cysteine protease caspase family. Caspases have a conserved pathway of regulators, including the pro-apoptotic Apaf-1, the antiapoptotic Bcl-2, and the proapoptotic BH-3 only in mammals (7-9). Recently, several forms of non-apoptotic regulated cell death have come to light (10) and their detailed mechanisms currently being elucidated, thereby adding to our knowledge of targets for treatment of human disease relevant to cell death.

In addition to the actual killing of cells fated to die, their remains must be efficiently removed via phagocytosis to avoid secondary necrosis and autoimmune consequences (11, 12). The mechanism of phagocytosis of apoptotic corpses has also been heavily studied, describing the molecular mechanisms of corpse engulfment, specifically in how dying cells are recognized (13) and how the phagocyte slated to be internalized extends around this corpse (14) and how, once fully internalized and encapsulated in a phagocytic vesicle called a phagosome, the corpse is eventually resolved through multiple steps of increased acidification of the phagosome (15) and introduction of lysosomal hydrolases (16). Apoptotic clearance is also well-known to occur via conserved pathways for engulfment and phagosome maturation following the complete internalization of the corpse (17, 18).

Much has been described in terms of cell killing and clearance at the molecular level using the powerful genetic model organism, the nematode *C. elegans* and the *C. elegans* germline (apoptosis) and male-specific linker cell (non-apoptotic LCD) have been informative settings to gain insights on PCD. Discoveries include the first description of the genetic regulation of apoptosis (19) and the discovery of a non-apoptotic form of cell death, Linker cell-type death (LCD) with conserved morphological features and genetic regulation (20). Phagocytosis has also been extensively characterized in the nematode, with seminal work done on corpse engulfment (21), the delineating of the molecular machinery and cell biology behind phagosome maturation (22). Newer studies include those describing roles in neuronal sculpting

71 and function (23), roles of LC3 lipidation in polar body removal (24) and multiple roles of the GTPase
72 RAB-35 in both apoptotic ell clearance and clearance following LCD (25, 26)
73 One regulator of both apoptotic and non-apoptotic (LCD) forms of PCD identified in *C. elegans* is
74 EOR-1, the ortholog the BTB/zinc-finger tumor suppressor transcription factor PLZF (27). In a non-cell
75 death context, EOR-1 is known to be involved in neuronal specification (28). In terms of PCD, EOR-
76 1/PLZF has been implicated both in apoptotic death of the HSN neurons (27) and the non-apoptotic
77 Linker-type Cell Death (LCD) (29). EOR-1 appears to play a specification role upstream to the execution
78 phase of these deaths acting upstream or in parallel to CED-9 in the HSNs and upstream of HSF-1 in
79 conjunction with WNT signaling in LCD (27). However, its precise mechanistic contribution to either form
80 of PCD remains unknown.
81 In addition to the core apoptotic gene regulation components, an additional regulator linked
82 specifically to germline apoptosis include the homolog of the mitochondrial flavoprotein, the Apoptosis
83 Inducing Factor AIF homolog, WAH-1(30, 31). Mammalian AIF is a multifunctional enzyme with essential
84 roles for both mitochondrial physiology and the elimination of dying cells (32). In *C. elegans*, WAH-1/AIF
85 has been associated separately with apoptotic cell removal at the level of both corpse recognition (30)
86 and DNA degradation (31).
87 We present here our application of an additional setting for PCD for specialized cells in *C. elegans*
88 in providing mechanistic insights into the genetic regulation and subcellular dynamics involved in different
89 steps of programmed cell elimination. We have previously described the tripartite cell killing program,
90 Compartmentalized Cell Elimination (CCE) of the scaffolding tail-spike epithelial cell (TSC) in the *C.*
91 *elegans* embryo, (33). Briefly, CCE entails three morphologically distinct cell elimination events that occur
92 in an ordered and morphologically stereotyped manner. The CCE program occurs 10 times slower than
93 most nematode cells fated to die apoptotically allowing for detailed examination of these events at the
94 gross and subcellar level (33). During CCE, the single process of the TSC segments into two
95 morphologically distinct sub-compartments that exhibit degenerative morphologies resembling two
96 different forms of neurite pruning (33). The soma appears to round, superficially resembling apoptotic
97 morphology (33). Owing to the distinct morphological profile of CCE, the demise of the TSC can serve as
98 a timekeeper for different events of cell elimination, both at the level of killing and clearance.
99 At the molecular level, CCE is genetically disparate from apoptosis (34-36). While it does require
100 the *C. elegans* caspase CED-3, it is not regulated by the homolog of BH3 only, the cell-specification factor
101 EGL-1/BH3-only (36). Multiple non-canonical regulators of CCE have been identified for cell killing (34-
102 36) In addition, we have found that the canonical engulfment machinery operates only on the soma
103 corpse (33), and that the process remnants require the cell-cell fusogen EFF-1 for autofusion of the newly
104 forming phagosome for phagosome closure (33). Thus, CCE is a promising system for generating new
105 insights into the molecular and cell biological machinery of programmed cell elimination.

106 In the present study, we leverage CCE as a morphologically and temporally well-defined, easily
107 scorable, program to define a specific role of EOR-1/PLZF in the regulation of *wah-1*/Aif in promoting
108 PCD. We describe defined spatiotemporal dynamics of WAH-1 as part of its dual sequential roles in cell
109 corpse internalization and resolution. We also describe a corpse progression transition state seen upon
110 failure of EOR-1/PLZF and WAH-1/AIF function. Our molecular and cell biological findings are highly
111 relevant for neurodegeneration, metabolic disease and cancer biology studies and our work presents
112 CCE as a viable setting to study new facets of the genetics and cell biology of programmed cell
113 elimination.
114
115 **Results**
116 **The transcription factor EOR-1/PLZF promotes CCE compartment-specifically**
117 We have previously described a highly ordered and organized tripartite developmental cell death
118 program, Compartmentalized Cell Elimination (CCE), in the nematode *C. elegans* (33). We have
119 observed CCE in two polarized cell types in the embryo, the scaffolding tail-spike epithelial cell (TSC)
120 and the sex-specific CEM sensory neurons(33). During CCE, these cells show three disparate regressive
121 morphologies. Both the TSC **(Figure 1A**) and the hermaphrodite CEMs extend a single process/dendrite
122 when intact (IMA, intact, mature). During early CCE (BA, beading, attached; BD, beading, detached), the
123 single process/dendrite shows axon pruning-like morphology proximally and axon retraction-like pruning
124 distally (**Figure 1B**). At this time, the soma rounds in a manner superficially resembling apoptotic cell
125 death. Later in CCE, the distal process retracts into a distal node (**Figure 1C**) (soma, distal retraction,
126 SDR) leaving behind a soma and a distal remnant (soma, distal degrading, SDD) (**Figure 1D**) which are
127 phagocytosed stochastically by different neighboring phagocytes before the animal hatches. The highly
128 organized and stereotyped elimination sequence of CCE allows us to use the cell's general morphology
129 as a time-keeper for events in this cell death program.
130 While CCE is dependent on the main *C. elegans* caspase CED-3 (33) it is genetically distinct from
131 apoptosis as it does not require EGL-1/BH-3-only (36) CCE is also temporally distinct from apoptosis as
132 it takes longer to complete. While most cells fated to die apoptotically in *C. elegans* live for only 30
133 minutes (37), the TSC lives for 5 hours (38) with CCE of the TSC taking 150 minutes (33). This longer
134 time-scale positions CCE of the TSC as a promising platform to better understand the fundamental cell
135 biology of programmed cell elimination in greater detail.
136 Bearing this in mind and leveraging the facile genetics of *C. elegans*, we performed a forward
137 genetic screen for CCE defects of the TSC using a membrane marker strain for the TSC (TSC-myrGFP)
138 we have previously employed (33). We obtained a mutant, *ns957,* bearing an inappropriately persisting
139 and enlarged cell body only, but with no process **(Figure 1E)**. This CCE defect increased when animals
140 were raised and scored at 25°C when compared to 20°C **(Figure 1 F)**.

141 Intrigued by a mutant where only soma elimination fails but where the process is successfully
142 eliminated, we examined the morphology of our mutant more carefully using Differential Interference
143 Contrast (DIC) microscopy. Apoptotic cell death has well-documented morphological characteristics that
144 are visible under DIC microscopy, such as pyknotic nuclei and refractility (39). However, we observed in
145 our *ns957* mutant enlarged and non-pyknotic nuclei, and a non-refractile cytoplasm (**Figure 1G-G"**).
146 Following Whole Genome Sequencing, genomic DNA rescue (**Figure 1 I**), and examination of
147 other alleles (**Figure 1J,K-K'**), we found that our screen mutant has a causative lesion of E570K in the
148 gene encoding the transcription factor EOR-1/PLZF (**Figure 1H**). We also found from cell-specific rescue
149 experiments that *eor-1* acts cell-autonomously in the TSC (**Figure 1L**) and that eor-1 is expressed in the
150 (**Figure 1 M**).
151
152 **EOR-1/PLZF acts downstream of CED-3/Caspase, but with known regulatory partners**
153 We proceeded to examine the precise role of EOR-1 in PCD using CCE of the TSC as our model.
154 In its known roles in cell fate, EOR-1 functions with known co-regulators of transcription. We first
155 examined for a role of EOR-2, which binds to the BTB domain of EOR-1 and promotes it function, (40)
156 by looking at *eor-2 (cs42)* mutants (**Figure 2A, B, C**) and found this to phenocopy *eor-1* mutants. EOR-
157 1/PLZF has also been reported to act as a pioneer transcription factor that functions in conjunction with
158 the MAU-2 cohesin loader, and the SWSN-1 SWI/SWNF chromatin remodeling complex member to
159 modify chromatin architecture and gene expression of genes required for the maturation of the post-
160 mitotic development of the HSN neurons (28). To determine whether EOR-1 functions with MAU-2 and
161 SWSN-1 to promote CCE, we examined *mau-2 (qm160)* **(Figure 2 A,D, E*)*** and *swsn-1 (ku355)* **(Figure**
162 **2 A,F, G)** mutant larvae and found that they show persisting TSC somas that phenocopy the distinct
163 morphology of *eor-1* mutant animals. Therefore, EOR-1 functions in the new setting of CCE via its
164 previously identified partners in transcription.
165 We next asked whether EOR-1 functions upstream or downstream of CED-3/caspase and
166 whether it impacts TSC fate in a more general way. As in the case of apoptosis, CCE requires the main
167 *C. elegans* caspase CED-3, as well as it's upstream regulator CED-4/Apaf1(36). We generated a *ced-*
168 *4(n1162); eor-1(cs28)* double mutant and found an intact TSC phenotype and nuclear phenotype
169 characteristic of *ced-3(n717)* single mutants (N=10/10), suggesting that EOR-1 acts downstream of CED-
170 4 and CED-3 to promote CCE and likely does not affect TSC development **(Figure 2H-H', I-I').**
171
172 **EOR-1/PLZF is important late in CCE for corpse internalization**
173 We next asked what aspect of CCE EOR-1 regulates. Given the striking soma morphology of *eor-*
174 *1* mutants, we examined closely the soma morphology changes across the different CCE stages in both
175 wild-type and *eor-1 (cs28)* mutants using a combination of DIC optics and our fluorescent TSC membrane

176 reporter. We noted down features of the TSC soma at different CCE stages. Prior to CCE, when the cell
177 has matured, but is still intact (Intact mature stage, IMA) (**Figure 3A-B"**), the soma appears polygonal
178 with its nuclei appearing ovoid, flat and speckled with many small refractile bodies (**Figure 3B'-B"**). As
179 CCE sets in, the soma becomes round and the proximal process displays beading (Beading attached
180 stage, BA) (**Figure 3C-D"**), during which the nuclei appear round and spheroid (**Figure 3D'-D"**). Nuclear
181 contents retain a speckled appearance of refractile material.

182 As CCE progresses to the next stage (soma-distal process retracting stage, SDR) (**Figure 3E-**
183 **F'**), the junction between the rounded soma is detached from the beading proximal process (**Figure 3E**)
184 and the distal process starts to retract into a node. At this stage, nuclei are rounded with intranuclear
185 contents beginning to condense into more discrete areas (**Figure 3F'-F"**). The soma and distal process
186 are the removed by separate phagocytes. At this stage, the soma forms a classical refractile, button-like,
187 appearance as it is starting to be engulfed. After the SDR/retraction stage, the soma and process appear
188 superficially to be degrading (Soma-distal process degrading stage, SDD) (**Figure 3G-H"**). The soma at
189 this point appears non-refractile and vacuolized, with its nuclei appearing pyknotic and detached **(Figure**
190 **3 H'-H"**). Apoptosis and other forms of PCD are defined by subcellular hallmarks such as specific
191 changes in nuclear morphology and cell enlargement. We find that, during CCE, pyknotic nuclei appear
192 also to exhibit Brownian motion within the non-refractile cytoplasm **(Figure 3H'-H"**). The TSC membrane
193 appears diffuse at this stage and the membrane loses its discrete ring surrounding the cell. We examined
194 *eor-1 (cs28)* TSC in a similar manner and found that CCE progression appeared normal up until the
195 SDD/soma-distal process degrading stage, where the nuclei fail to condense and the membrane does
196 not lose its integrity (**Figure 3I-P"**).

197 To better characterize the soma persistence defect of *eor-1 (ok1127)* mutants, we compared the
198 mutant defect with that of mutants for caspase/cell killing, *ced-3(n717)* and engulfment, *ced-12 (ky149),*
199 and performed epistasis. We compared the soma-persistence defects of *ced-3 (n717)* (**Figure 4 A-A"**)
200 and *ced-12(ky149)* mutants (**Figure 4 B-B"**) and *eor-1*(**Figure 4 C-C"**). We observed that the TSC soma
201 morphological features of *eor-1* were distinct from both *ced-3 (n717)* and *ced-12(ky149)* mutants
202 suggesting the cell is neither living nor engulfed. Moreover, a double mutant for *eor-1* and *ced-12 (ky149)*
203 (**Figure 4D -D"**) phenocopied the *eor-1 (ok1127)* single mutants, rather than the refractile corpse of *ced-*
204 *12 (ky149)* mutants. This supports the idea that the persisting soma of *eor-1* mutants has progressed
205 through the killing steps of CCE but has not been engulfed and is consistent with an arrest at the SDD
206 stage. We proceeded to examine whether the persisting corpse of *eor-1 (cs28)* mutants is internalized
207 by its neighboring phagocyte. We used a cytosolic reporter labelling the TSC soma's neighboring
208 phagocyte (*skn-1p*::mKate2) and found that the persisting soma *eor-1* **(Figure 4 E-G; Supplemental**
209 **Movie S1**) mutants remains outside the phagocyte *(*N=10/12*),* suggesting failure of corpse
210 internalization.

211
212
213 **EOR-1/PLZF positively regulates *wah-1*/Aif expression in the TSC**
214 We next sought to identify the transcriptional target for EOR-1/PLZF in the context of CCE and
215 examined published data obtained from a previous ChiP-Seq analysis study of EOR-1/PLZF
216 transcriptional targets (41). We caught note of the gene *wah-1* which encodes WAH-1, the homolog of a
217 mitochondrial flavoprotein, the Apoptosis Inducing Factor AIF1 homolog, a multifunctional enzyme that is
218 essential for mitochondrial bioenergetic function (32). Interestingly WAH-1 has been shown to function to
219 promote apoptotic cell death in the *C. elegans* germline (31). Upon activation by CED-3/Caspase and
220 EGL-1/BH3-only, WAH-1/AIF promotes apoptosis by through DNA degradation via the CPS-6
221 endonuclease (31). WAH-1/AIF has also been shown to aid in phosphatidylserine (PS) exposure by
222 promoting SCRM-1 scramblase function (30) to facilitate apoptotic corpse recognition.
223 We tested the hypothesis that EOR-1/PLZF promotes CCE through the transcriptional activation
224 of *wah-1*. First, we looked at a mutant for *wah-1* in the TSC-myrGFP background. We found *wah-1*
225 (*gk5392*) mutants to phenocopy *eor-1* mutants (**Figure 5A, B**), and the double mutant not additive
226 (**Figure 5B**). We also found from cell-specific rescue experiments that *wah-1* functions in the TSC (**Figure**
227 **5C)**. We examined an endogenous reporter for *wah-1* (*wah-1* promoter driven WAH-1::GFP) at the intact
228 mature (IMA) embryo stage in wild-type (**Figure 5D)**, *eor- 1(cs28)* (**Figure 5E**), *mau- 2 (gm160)*(**Figure**
229 **5F)**, and *swsn-1(os22)* (**Figure 5G**) mutants and found decreased levels of *wah-1* expression in
230 mutants(**Figure 5H**). These data support the notion that WAH-1 promotes CCE by acting within the TSC
231 and is transcriptionally regulated by EOR-1, MAU-2 and SWSN-1. This is supported by modENCODE
232 data for *wah-1* identifying an EOR-1 binding sequence at the *wah-1* promoter(42). Further, *wah-1*
233 contains an HTZ-1 histone binding site, further supporting the involvement of a chromatin remodeling
234 complex in maintaining *wah-1* transcription as cohesin loaders require nucleosome-free loci to bind.
235
236 **WAH-1 functions in corpse internalization**
237 We first considered WAH-1's possible role at the plasma membrane, as the soma rounds, and
238 presumably about to be engulfed. Prior studies have shown that WAH-1/AIF promotes apoptotic corpse
239 recognition, and engulfment (30). We looked at CCE progression in *wah-1* (gk5392) (**Figure 6 A-H"**)
240 mutants and found that the progression differed from wild-type, arresting, as in *eor-1* mutants, at the SDD
241 stage (**Figure 6 G-H"**).
242 Next, we used a cytosolic reporter labelling the TSC soma's neighboring phagocyte (*skn-*
243 *1*p::mKate2) and found that the persisting soma of *wah-1* mutants remains outside the phagocyte **(Figure**
244 **6I-K**) (N=11/13), also similar to *eor-1* mutants. We also noted that in both *eor-1* and *wah-1* mutants the
245 phagocyte pseudopods are not formed (**Figure 4E-G, Supplemental Movie S1; Figure 6I-K;**

246 **Supplemental Movie S2**), suggesting failure in corpse recognition. This contrasts with from our previous
247 work showing that mutations for the phagosome sealing fusogen gene *eff-1* do have extended
248 pseudopods and can recognize the TSC process remnants, though the phagosome cannot close (33).
249 WAH-1 has been shown to promote SCRM-1 scramblase flipping of phosphatidyl serine from the
250 inner to the outer plasma membrane (30). We found that mutants for *scrm-1(-)* also displayed CCE
251 defects (**Figure 6 L, M)** akin to *eor-1* and *wah-1* mutants. These data suggest WAH-1 is important for
252 TSC soma corpse recognition during CCE in a manner dependent of SCRM-1 as seen in its apoptotic
253 role.
254
255 **WAH-1 also functions in nuclear dismantling after corpse internalization**
256 WAH-1 has been previously shown to be involved in DNA degradation and is reported to
257 translocate from the mitochondria to the nucleus (31). How this correlates to the role at the plasma
258 membrane has not been determined. We attempted to address this both genetically and cell biologically
259 in the context of TSC elimination. We first tested whether in the context of CCE WAH-1 indeed functions
260 in DNA degradation and how this may impact the exaggerated nuclear morphology of *wah-1* and *eor-1*
261 mutants. To this end, we attempted to separate WAH-1 function in corpse internalization versus its
262 possible nuclear role.
263 WAH-1 has been shown to promote DNA degradation during apoptosis by acting to enhance the
264 activity of the CPS-6/Endonuclease G nuclease (31, 43). We found that *cps-6* mutants also phenocopy
265 *wah-1* and *eor-1* mutants for CCE (**Figure 7A, B).** Moreover, a *wah-1; cps-6* double mutant did not show
266 an increase in TSC defects (**Figure 7A**) suggesting these genes function in the same genetic pathway.
267 We also found that mutants for *nuc-1*, a lysosomal acid hydrolase that promotes late DNA degradation
268 (44, 45), also phenocopy *eor-1* and *wah-1* mutants (**Figure 7A, C)** supporting a role for WAH-1 in DNA
269 degradation. Interestingly, it has been reported that degradation of DNA of apoptotic cell corpses requires
270 contributions of both the dying and the engulfing cell(45). NUC-1 has been shown to be released from
271 the apoptotic corpse into the phagolysosome allowing for DNA degradation.
272 We next investigated whether *cps-6* mutants were arrested at a phagosome maturation stage.
273 We looked at whether the soma of *cps-6* mutants is internalized, which we would expect if the loss of
274 CPS-6 affects a post-engulfment stage as the phagosome-containing the internalized corpse matures.
275 Interestingly, unlike for *wah-1* and *eor-1*, the soma of *cps-6* mutants appears to be internalized (**Figure**
276 **7D-F; Supplemental Movie S3**) (N=9/10), suggesting that CPS-6/EndoG is not involved in WAH-1's
277 corpse internalization function and rather likely plays its role in nuclear degradation downstream of
278 internalization during phagosome maturation to resolve the internalized corpse.
279 To test which stage of phagosome maturation WAH-1 and CPS-6 may function in nuclear
280 disintegration, we looked at known markers the sequential steps of phagosome maturation. We looked

281 at phagosomal markers for early (GFP::RAB-5) (**Figure 7G-G''**), late (GFP::RAB-7) (**Figure 7H-H''**) and
282 phagolysosomes (LAAT-1::mCherry) (**Figure 7I-I''**)(33) in *cps-6* mutants and found that the phagosome
283 bearing the internalized corpse is decorated by LAAT-1, suggesting arrest at the phagolysosomal stage.
284 This is consistent with a role of NUC-1 in TSC DNA degradation and supports NUC-1 as being a
285 phagolysosomal substrate. This also suggests a defect in corpse degradation causes the dramatic
286 nuclear and cytoplasmic phenotypes in mutants.
287

288 **Defined spatiotemporal dynamics suggest dual functions of WAH-1/AIF before and after corpse**
289 **internalization**

290 Having identified WAH-1/AIF as a regulator of CCE at both the level of corpse internalization and
291 degradation, we next examined its localization pattern of across CCE stages (**Figure 8)**. We first
292 examined TSC promoter-driven WAH-1::mCherry against a TSC promoter-driven mitochondrial matrix
293 marker (**Figure 8A-D**). When the cell is intact, WAH-1 appears to be mitochondrial (**Figure 8A**) and not
294 in the plasma membrane. However, as the beading (BA/BD) stage begins and the soma rounds and has
295 detached from the process mitochondria and WAH-1 both appear to be at or close to the plasma
296 membrane (**Figure 8 B, C**). Afterwards, at the SDD stage, WAH-1 is not seen at the plasma membrane
297 but can be seen in what appears to be fragmented mitochondria but is largely delocalized and cytoplasmic
298 (**Figure 8D**). To better understand this localization pattern, we examined TSC mitochondrial localization
299 against the TSC plasma membrane. Interestingly, we found mitochondria to be close to the plasma
300 membrane through most of CCE (**Figure 8E, F, G**), appearing fragmented at the SDD stage when the
301 plasma membrane integrity is lost (**Figure 8H**).

302 We next attempted to position the TSC soma during the SDD stage relative to its phagocyte to
303 further assess WAH-1's role. In order to use the distinct morphology of CCE steps to temporally trace the
304 status of the TSC soma as it progresses through CCE, we imaged our TSC reporter against the soma-
305 phagocyte reporter in wild-type embryos (**Figure 8I-W)**. As expected, the TSC soma is seen outside the
306 phagocyte at the IMA stage (**Figure 8I-L)** We found that the TSC soma is internalized from what we
307 define as the BD (beading, detached) stage when the soma rounds and appears refractile (**Figure 8M-**
308 **P**) through the SDR (**Figure 8Q-T**) and SDD (**Figure 8U-X**) stages. We observe WAH-1 outside of
309 mitochondria at the SDD stage (**Figure 8 D** and **8U-X**) after being at the mitochondria and plasma
310 membrane earlier at the SDR (**Figure 8 C** and **8Q-T**) and BD (**Figure 8 B** and **8M-P**) stages. Together,
311 these data suggest that a physical association between mitochondria and the plasma membrane, that
312 may involve WAH-1, may be important early in phagocytosis and that exit of WAH-1 from mitochondria
313 may be important for corpse degradation and digestion after internalization.
314

315 **Discussion**

316 Here we describe defined subcellular events of a developmentally killed cell as it progresses
317 through the sequential steps of phagocytic clearance. Our work supports a model in which WAH-1/AIF
318 dual function, positively regulated by transcriptional control by EOR-1/PLZF, ensures clearance of the
319 TSC corpse as a feature of CCE. We show that WAH-1/AIF is localized sequentially at very specific
320 stages of CCE that promote different phagocytic events, corpse internalization and, shown for the first
321 time in this study, corpse resolution during phagosome maturation when the corpse is in the
322 phagolysosome. We propose that this two-step role of WAH-1/AIF allows for controlled cellular demise
323 of the TSC soma. We provide an expanded cell biological and genetic characterization of CCE in *C.*
324 *elegans*, by assigning a specific and previously unidentified role *in vivo* for EOR-1/PLZF in the regulation
325 of *wah-/Aif1*. Our study expands on our knowledge of the contribution of WAH-1 on PCD by providing
326 spatial and temporal contexts for its function in CCE. Additionally, we present previously unreported
327 persisting cell corpse features in *C. elegans* during the failure of EOR-1/PLZF and WAH-1/AIF function.
328 CCE events are compartment-specific with different factors regulating the demise and removal of different
329 subcellular compartments (33). We find that WAH-1 and EOR-1 are also compartment-specific regulators
330 that impact only the removal of the soma, which is consistent with a role in DNA degradation and nuclear
331 changes. Our study expands on prior studies linking EOR-1/PLZF to apoptotic (27) and non-apoptotic
332 (29) PCD by providing a precise mechanistic contribution of EOR-1/PLZF in the context the CED-
333 3/caspase dependent but genetically non-apoptotic CCE program and provide evidence supporting that
334 WAH-1/AIF is an *in vivo* target of EOR-1/PLZF. We also introduce here a new corpse transition state
335 during when the cell elimination program is compromised, and propose that, just as killing, programmed
336 cell degradation must occur in a controlled highly regulated manner, not just via catastrophic destruction.
337 We propose that by regulating when DNA degradation and nuclear destruction takes place the corpse
338 facilitates its own controlled degradation in response to the conditions of the phagolysosomal
339 pH/enzymatic microenvironment.
340 Additionally, WAH-1/AIF studies to our knowledge have been limited to the *C. elegans* germ cell
341 apoptosis. During apoptosis, WAH-1's mitochondrial origin (31) and role in corpse recognition (30) and
342 as a nuclease (31) have been described. Here we describe its role in a genetically non-apoptotic program
343 and capitalizes on the longer time scale of CCE to capture sequential spatiotemporal dynamics of WAH-
344 1 within the cell corpse as it progresses through phagocytosis stages and correlate the cell's
345 microenvironment with WAH-1's localization and function. Future studies on WAH-1 dynamics and
346 function for other forms of PCD such as LCD would be of great interest to the field. It will be interesting
347 to explore whether the same transcriptional relationship between EOR-1 and *wah-1* exist in these other
348 forms of PCD.
349 Notably, WAH-1 exit from mitochondria is reported to be dependent on EGL-1 (31). However,
350 CCE, while CED-3/caspase-dependent, is independent of EGL-1/BH3-only (36). The WAH-1 localization

351 pattern suggests WAH-1 can promote nuclear degradation independent of EGL-1, even though it is
352 thought that WAH-1 may be translocated to the nucleus by EGL-1. The lack of EGL-1 involvement may
353 affect WAH-1's ability to be released from mitochondria and may explain why WAH-1 is still associated
354 to some degree with mitochondria until the SDD stage of CCE. The lack of EGL-1 may cause WAH-1's
355 mitochondrial release to be markedly slower, which may explain why the time course of CCE is much
356 longer than apoptotic germline cells. Of note, the TSC serves in tail scaffolding as the embryo develops
357 (33) and must therefore persist until this it completes this function, making it one of the more long-lived
358 cells programmed to die.
359 Our work also opens up several exciting questions for future exploration. It is known that WAH-
360 1/AIF is an important mitochondrial factor(32), but it is unclear what guides its translocation to the plasma
361 membrane and nucleus in a temporally regulated manner. Whether phosphatidyl serine is exposed during
362 CCE is also yet to be addressed. Also of interest is the molecular mechanism by which WAH-1/AIF
363 perceives the changing phagosomal environment and responds by translocating to the nucleus to
364 execute its role in DNA and nuclear degradation. How does WAH-1/AIF know to translocate so specifically
365 in the corpse at distinct phagosomal stages? We also suggest that failure to appropriately degrade DNA
366 can lead to not only cell persistence but severe exaggerations in nuclear morphology. From our study,
367 failure of DNA degradation whether the corpse is outside or inside the phagocyte leads to enlarged
368 nuclear size. What is the intrinsic signal for this nuclear enlargement? How aberrant DNA stability
369 translates to structural changes in the nucleus is also an interesting avenue to explore. Unexpectedly, we
370 observed that the DIC and TSC membrane marker phenotypes of *eor-1*, *wah-1*, *scrm-1*, and *cps-6*
371 mutants appear superficially similar (persistent enlarged soma with exaggerated nuclei), though we find
372 only *cps-6* mutants to have internalized corpses. Further genetic screens may identify factors affecting
373 nuclear shape and size that may resolve this surprising observation. Taken together, our study further
374 solidifies CCE as a powerful system to offer new insights on the genetics and cell biology of programmed
375 cell killing and clearance.
376
377 **Materials and Methods**
378
379 ***C. elegans* methods**
380 *C. elegans* strains were cultured using standard methods on *E. coli* OP50 and grown at 20ºC. Wild-type
381 animals were the Bristol N2 subspecies. For most TSC experiments, one of two integrated reporters were
382 used: *nsIs435=TSCp::myrGFP* or *nsIs685=TSCp::mKate2-PH.* In addition, *nsIs650=wah-1*p::WAH-
383 1::GFP was used. Integration of extrachromosomal arrays was performed using UV and trioxsalen
384 (T2137, Sigma). Animals were scored at 20ºC, unless otherwise mentioned.
385

386 **Imaging**

387 Images were collected on a Nikon TI2-E Inverted microscope using a CFI60 Plan Apochromat Lambda
388 60x Oil Immersion Objective Lens, N.A. 1.4 (Nikon) and a Yokogawa W1 Dual Cam Spinning Disk
389 Confocal images were acquired using NIS-Elements Advanced Research Package. For still embryo
390 imaging, embryos were anesthetized using 0.5 M sodium azide. Larvae were paralyzed with 10mM
391 sodium azide. Widefield imaging was performed on a Carl Zeiss Axio Imager.M2 microscope with 63X oil
392 immersion lens. Super-resolution images were taken using a VTiSIM Super resolution Live Cell Confocal
393 Imaging System.

394

395 **Quantifying CCE defects**

396 TSC death defects were scored at the L1 stage. Animals were mounted on slides on 2% agarose-M9
397 pads, paralyzed with 10mM sodium azide, and examined on a Carl Zeiss Axio Imager.M2 microscope
398 with 63X oil immersion lens. The persisting TSC was identified by fluorescence based on its location and
399 morphology. At least 50 animals were scored per genotype. For images, each image is representative of
400 10 sampled.

401

402 **Worm strains used in this study—**

403 List gene alleles under different chromosomes linkage groups (LG I-X)

404 LGI: *ced-12(ky149), mau-2(qm160), scrm-1(tm698), cps-6(ok1718)*

405 LGII:

406 LGIII*: ced-4(n1162), wah-1 (gk5392)*

407 LGIV: *eor-1(ok1127), eor-1(cs28), ced-3(n717)*

408 LGV: *swsn-1(os22)*

409 LGX: *eor-2 (cs42) nuc-1 (e1392)*

410

411 **Plasmids and Transgenics**

412 Plasmids were generated via Gibson cloning. Primer sequences and information on the construction of
413 plasmids used in this study are provided in (Supplemental Table 1). The full list of transgenes is described
414 in (Supplemental Table 2). The full length or fragment of the *aff-1* promoter was used to label the TSC.

415 **Quantification of WAH-1::GFP fluorescence intensity**

416 Images of the intact TSC in animals harboring *wah-1* promoter driven *wah-1*::GFP in WT, *eor-1(cs28)*,
417 *mau-2(qm160)*, and *swsn-1(os22)* were collected using confocal microscopy as stated above using the
418 same settings across all images. Sum intensity projections of the TSC soma were generated by following

TSCp::mCherry in Fiji Image J software and GFP intensity was then calculated using this software. CTCF was calculated and graphed using Graphpad. All data points represent the average of 10 animals. Statistical significance was determined by Mann-Whitney U test for comparison between wild type and mutant animals.

Statistics

Sample sizes and statistics were based on previous studies of CCE and the TSC(33). Independent transgenic lines were treated as independent experiments. An unpaired two-tailed *t*-test was used for all persisting TSC quantifications (GraphPad Prism). For all figures, mean ± standard error of the mean (s.e.m.) is represented. P-values are indicated in (Supplemental Table 3)

Acknowledgments:

NR and PG designed the experiments and wrote the manuscript. NR, MW, KJ, RS, performed the experiments. GC provided significant technical assistance. *ns957* was isolated by PG and MW in the laboratory of SS. We thank members of the Ghose lab for comments on the manuscript. Some strains were provided by the CGC, which is funded by NIH Office of Research Infrastructure Programs (P40 OD010440).

Funding:

PG is a Cancer Prevention Research Institute of Texas (CPRIT) Scholar in Cancer Research (RR100091) and is also funded by a National Institutes of Health-National Institute of General Medical Sciences Maximizing Investigators' Research Award (MIRA) (R35GM142489). NR was supported by NIH SURF Supplemental Award 3R35GM142489-02S2. KJ was funded by NIH Diversity Supplement Program Award 3R35GM142489-02S1, 3R35GM142489-03S1. MW received funding from The Rockefeller University Summer "Gateways to The Laboratory' Program. SS was funded by NIH grants R01HD103610 and R35NS105094.

Figure Legends:

Figure 1. EOR-1/PLZF promotes CCE cell-autonomously. (A-D) Stages of CCE**.** IMA, intact mature cell; BD, beading, detached; SDR, soma-distal retracted; SDD, soma, distal degrading. n = 10 biologically independent animals each with similar results. **(E)** Mutant *ns957* at L1 stage showing persisting TSC soma. n = 10 biologically independent animals each with similar results **(F)** Quantification of *ns957* CCE defects. Data are mean +/_ s.e.m. Statistics: Anova, see Supplementary Table 3 for individual P values. **G-G'')** Enlarged view of *ns957* persisting soma to show DIC view. **(I)** Gene structure of *eor-1*. **(J)**

454 Quantification of *eor-1* fosmid DNA rescue of *ns957*, n=50. (**K)** Quantification CCE defects of other *eor-*
455 *1* alleles, n=150. **(L, L')** Quantification of CCE defects of additional *eor-1* mutant alleles. **(M)** *eor-1* TSC-
456 specific rescue, n=150. **(N)** *eor-1* expression, *eor-1* promoter-driven mKate2. n = 10 biologically
457 independent animals each with similar results**.** Scale bar, 5 μm. Data are mean +/ s.e.m. Statistics: Anova
458 and two-tailed unpaired student's t-test, see Supplementary Table 3for individual P values.
459
460 **Figure 2. EOR-1/PLZF functions in CCE with its known partners but likely downstream of CED-**
461 **3/Caspase. (A)** CCE defects across *eor-1* alleles and *eor-2*, *mau-2* and *swsn-1* mutants. Persisting TSC
462 soma phenotypes in **(B, C)** *eor-2(cs42)*, **(D, E)** *mau-2 (qm160)* n = 10 biologically independent animals
463 each with similar results and **(F, G)** *swsn-1 (ku355)* n = 5 biologically independent animals each with
464 similar results. The TSC remains intact at L1 in both *ced-3 (n717)* **(H)** and *ced-4 (n1162)); eor-1(cs28)* **(I)**
465 n = 10 biologically independent animals each with similar results**.** Scale bar, 5 μm. n=150 for statistics.
466 Data are mean +/_ s.e.m Statistics: two-tailed unpaired student's t-test, see Supplementary Table 3 for
467 individual P values.
468
469 **Figure 3. Loss of EOR-1/PLZF causes corpse arrest late in CCE progression.** CCE of TSC
470 (membrane marker) in wild-type (**A-F"**) and *eor-1(cs28)* (**I-P"**) mutants showing progression of soma
471 elimination. Left-most panels show whole cell. (**A-B"**) IMA stage in wild-type. n = 10 biologically
472 independent animals each with similar results, (**C-D"**) BA stage in wild-type, n = 8 biologically
473 independent animals each with similar results, (**E-F"**) SDR stage in wild-type, n = 10 biologically
474 independent animals each with similar results, (**G-H"**) SDD stage in wild-type, n = 10 biologically
475 independent animals each with similar results. (**I-J"**) *eor-1 (cs28)* IMA n = 8 biologically independent
476 animals each with similar results, (**K-L"**) *eor-1 (cs28)* BA n = 6 biologically independent animals each with
477 similar results, (M-N") *eor-1 (cs28)* SDR n = 10 biologically independent animals each with similar results,
478 (**O-P"**) *eor-1 (cs28)* SDD n = 10 biologically independent animals each with similar results Scale bar, 5
479 μm.
480 **Figure 4. The cell corpse of *eor-1* mutants is not internalized by the neighboring phagocyte.**
481 Enlarged view of TSC soma at L1 in *ced-3(n717)* (**A-A"**), *ced-12(ky149)* (**B-B"**)**,** *eor-1(ok1127)* (C-C"),
482 *eor-1; ced-12* (**D-D"**), (**E-G**) Test for TSC soma corpse (green) internalization for *eor-1 (cs28)* mutant L1
483 *larvae* by phagocyte (magenta) at different planes of the phagocyte (upper , middle, lower). n = 10
484 biologically independent animals each with similar results. Scale bar, 5 μm.
485
486 **Figure 5.EOR-1/PLZF-1 positively regulates *wah-1*/Aif transcription to promote CCE. (A)** *wah-*
487 *1(allele)* CCE defect of TSC at L1 n = 10 biologically independent animals each with similar results. **(B)**
488 Quantification of *wah-1* mutant defect compared to *eor-1* and *wah-1; eor-1* double mutant. **(C)** Graph of

489 TSC-specific rescue of *wah-1* mutant phenotype. Endogenous *wah-1* expression intensity in wild-type
490 **(D)**, *eor-1* **(E)**, *mau-2* **(F)** and *swsn-1* **(G)** mutants. **(H)** Quantification of *wah-1* expression. n = 10
491 biologically independent animals each with similar results. Scale bar, 5 μm. Statistics: two-tailed unpaired
492 student's t-test for scoring and Mann Whittney U test for fluorescence intensity, see Supplementary Table
493 3 for individual P values.
494
495 **Figure 6. The cell corpse of *wah-1* mutants is not internalized and may function at the plasma**
496 **membrane. (A-H")** CCE progression in *wah-1(gk5392).* (**A-B"**) IMA *wah-1 (gk5392)* n = 4 biologically
497 independent animals each with similar results**,** (**C-D"**) BA *wah-1 (gk5392)* n = 5 biologically independent
498 animals each with similar results, (**E-F"**) SDR *wah-1 (gk5392)* n = 4 biologically independent animals
499 each with similar results, (**G-H"**) SDD *wah-1 (gk5392)* n = 3 biologically independent animals each with
500 similar results **(I-K)** TSC and soma-phagocyte dual marker strain in *wah-1* mutant L1 showing failure in
501 TSC corpse internalization. **(L)** L1 *scrm-1* mutant showing persisting TSC soma and exaggerated nuclei.
502 n = 10 biologically independent animals each with similar results. **(M)** Quantification of *scrm-1* mutant
503 defect. Scale bar, 5 μm. Statistics: two-tailed unpaired student's t-test, see Supplementary Table 3 for
504 individual P values.
505
506 **Figure 7. WAH-1 may promote nuclear degradation of the TSC soma corpse at phagolysosomal**
507 **stage. (A)** Quantification of *cps-6(ok1718)* and *nuc-1(e1382)* CCE defect of TSC (soma persistence) at
508 L1. **(B)** Images of these defects. **(D)** Test for soma corpse internalization for *cps-6(ok1718)* across
509 phagocyte planes (upper, middle lower)**.** Localization of phagocyte GFP::RAB-5 **(G-G"),** GFP**::**RAB-7 **(H-**
510 **H")** and LAAT-1:mCherry **(I'-I")** relative to TSC corpse of *cps-6(ok1718)* mutant at L1 stage. n = 10
511 biologically independent animals each with similar results. Scale bar, 5 μm. Statistics: two-tailed unpaired
512 student's t-test, see Supplementary Table 3 for individual P values.
513
514 **Figure 8. WAH-1 exhibits defined spatiotemporal dynamics during CCE progression correlated**
515 **with its function.** TSCp::WAH-1::mCherry and TSCp::mito::GFP localization during CCE IMA **(A**), BA
516 (**B**), SDR (**C**) and SDD (**D**) stages in wild-type embryos. TSCp::mKate2-PH (membrane) and
517 TSCp::mito::GFP localization during CCE IMA **(E**), BA (**F**), SDR (**G**) and SDD (**H**) stages in wild-type
518 embryos. Relative position of TSC soma versus soma phagocyte (upper, middle and lower phagocyte
519 planes) at different CCE stages, IMA (**I, J-L**), BD (**M, N-P**), SDR (**Q, R-T**) and SDD (**U, V-X**). n = 10
520 biologically independent animals each with similar results for A-D. Scale bar, 5 μm.
521
522 **Figure 9. Model.** EOR-1-regulated WAH-1 translocates to different TSC soma sub-compartments to
523 sequentially promote corpse internalization and resolution.

Supplemental Tables:

Supplemental Table 1. Plasmids used in this study.

Supplemental Table 2. Transgenes used in this study.

Supplemental Table 3. Statistics and P values.

Supplemental Movies:

Supplemental Movie S1. Test for TSC soma internalization of *eor-1 (cs28)* mutants. Green, TSC membrane, Magenta, phagocyte cytosolic marker.

Supplemental Movie S2. Test for TSC soma internalization of *wah-1* mutants. Green, TSC membrane, Magenta, phagocyte cytosolic marker.

Supplemental Movie S3. Test for TSC soma internalization of *cps-6* mutants. Green, TSC membrane, Magenta, phagocyte cytosolic marker.

References

1. Kerr JF, Wyllie AH, Currie AR. Apoptosis: a basic biological phenomenon with wide-ranging implications in tissue kinetics. Br J Cancer. 1972;26(4):239-57.
2. Nonomura K, Yamaguchi Y, Hamachi M, Koike M, Uchiyama Y, Nakazato K, et al. Local apoptosis modulates early mammalian brain development through the elimination of morphogen-producing cells. Dev Cell. 2013;27(6):621-34.
3. Lucantoni F, Salvucci M, Dussmann H, Lindner AU, Lambrechts D, Prehn JHM. BCL(X)L and BCL2 increase the metabolic fitness of breast cancer cells: a single-cell imaging study. Cell Death Differ. 2021;28(5):1512-31.
4. Wang Q, Wang Y, Ding J, Wang C, Zhou X, Gao W, et al. A bioorthogonal system reveals antitumour immune function of pyroptosis. Nature. 2020;579(7799):421-6.
5. Jolly PD, Smith PR, Heath DA, Hudson NL, Lun S, Still LA, et al. Morphological evidence of apoptosis and the prevalence of apoptotic versus mitotic cells in the membrana granulosa of ovarian follicles during spontaneous and induced atresia in ewes. Biol Reprod. 1997;56(4):837-46.
6. Saraste A, Pulkki K. Morphologic and biochemical hallmarks of apoptosis. Cardiovasc Res. 2000;45(3):528-37.
7. Zou H, Henzel WJ, Liu X, Lutschg A, Wang X. Apaf-1, a human protein homologous to C. elegans CED-4, participates in cytochrome c-dependent activation of caspase-3. Cell. 1997;90(3):405-13.

561 8. Vaux DL, Cory S, Adams JM. Bcl-2 gene promotes haemopoietic cell survival and cooperates
562 with c-myc to immortalize pre-B cells. Nature. 1988;335(6189):440-2.
563 9. Ohno H, Takimoto G, McKeithan TW. The candidate proto-oncogene bcl-3 is related to genes
564 implicated in cell lineage determination and cell cycle control. Cell. 1990;60(6):991-7.
565 10. Tait SW, Ichim G, Green DR. Die another way--non-apoptotic mechanisms of cell death. J Cell
566 Sci. 2014;127(Pt 10):2135-44.
567 11. Arandjelovic S, Ravichandran KS. Phagocytosis of apoptotic cells in homeostasis. Nat Immunol.
568 2015;16(9):907-17.
569 12. Poon IK, Lucas CD, Rossi AG, Ravichandran KS. Apoptotic cell clearance: basic biology and
570 therapeutic potential. Nat Rev Immunol. 2014;14(3):166-80.
571 13. Savill J, Fadok V, Henson P, Haslett C. Phagocyte recognition of cells undergoing apoptosis.
572 Immunol Today. 1993;14(3):131-6.
573 14. Park SY, Kim IS. Engulfment signals and the phagocytic machinery for apoptotic cell clearance.
574 Exp Mol Med. 2017;49(5):e331.
575 15. Lu N, Zhou Z. Membrane trafficking and phagosome maturation during the clearance of
576 apoptotic cells. Int Rev Cell Mol Biol. 2012;293:269-309.
577 16. Kinchen JM, Ravichandran KS. Phagosome maturation: going through the acid test. Nat Rev
578 Mol Cell Biol. 2008;9(10):781-95.
579 17. Fairn GD, Grinstein S. How nascent phagosomes mature to become phagolysosomes. Trends
580 Immunol. 2012;33(8):397-405.
581 18. Pauwels AM, Trost M, Beyaert R, Hoffmann E. Patterns, Receptors, and Signals: Regulation of
582 Phagosome Maturation. Trends Immunol. 2017;38(6):407-22.
583 19. Ellis HM, Horvitz HR. Genetic control of programmed cell death in the nematode C. elegans.
584 Cell. 1986;44(6):817-29.
585 20. Abraham MC, Lu Y, Shaham S. A morphologically conserved nonapoptotic program promotes
586 linker cell death in Caenorhabditis elegans. Dev Cell. 2007;12(1):73-86.
587 21. Ellis RE, Jacobson DM, Horvitz HR. Genes required for the engulfment of cell corpses during
588 programmed cell death in Caenorhabditis elegans. Genetics. 1991;129(1):79-94.
589 22. Guo P, Hu T, Zhang J, Jiang S, Wang X. Sequential action of Caenorhabditis elegans Rab
590 GTPases regulates phagolysosome formation during apoptotic cell degradation. Proc Natl Acad Sci U S
591 A. 2010;107(42):18016-21.
592 23. Raiders S, Black EC, Bae A, MacFarlane S, Klein M, Shaham S, et al. Glia actively sculpt
593 sensory neurons by controlled phagocytosis to tune animal behavior. Elife. 2021;10.
594 24. Fazeli G, Stetter M, Lisack JN, Wehman AM. C. elegans Blastomeres Clear the Corpse of the
595 Second Polar Body by LC3-Associated Phagocytosis. Cell Rep. 2018;23(7):2070-82.
596 25. Haley R, Wang Y, Zhou Z. The small GTPase RAB-35 defines a third pathway that is required
597 for the recognition and degradation of apoptotic cells. PLoS Genet. 2018;14(8):e1007558.
598 26. Kutscher LM, Keil W, Shaham S. RAB-35 and ARF-6 GTPases Mediate Engulfment and
599 Clearance Following Linker Cell-Type Death. Dev Cell. 2018;47(2):222-38 e6.
600 27. Hoeppner DJ, Spector MS, Ratliff TM, Kinchen JM, Granat S, Lin SC, et al. eor-1 and eor-2 are
601 required for cell-specific apoptotic death in C. elegans. Dev Biol. 2004;274(1):125-38.
602 28. Shinkai Y, Kuramochi M, Doi M. Regulation of chromatin states and gene expression during
603 HSN neuronal maturation is mediated by EOR-1/PLZF, MAU-2/cohesin loader, and SWI/SNF complex.
604 Sci Rep. 2018;8(1):7942.
605 29. Malin JA, Kinet MJ, Abraham MC, Blum ES, Shaham S. Transcriptional control of non-apoptotic
606 developmental cell death in C. elegans. Cell Death Differ. 2016;23(12):1985-94.
607 30. Wang X, Wang J, Gengyo-Ando K, Gu L, Sun CL, Yang C, et al. C. elegans mitochondrial factor
608 WAH-1 promotes phosphatidylserine externalization in apoptotic cells through phospholipid scramblase
609 SCRM-1. Nat Cell Biol. 2007;9(5):541-9.
610 31. Wang X, Yang C, Chai J, Shi Y, Xue D. Mechanisms of AIF-mediated apoptotic DNA
611 degradation in Caenorhabditis elegans. Science. 2002;298(5598):1587-92.

32. Troulinaki K, Buttner S, Marsal Cots A, Maida S, Meyer K, Bertan F, et al. WAH-1/AIF regulates mitochondrial oxidative phosphorylation in the nematode Caenorhabditis elegans. Cell Death Discov. 2018;4:2.
33. Ghose P, Rashid A, Insley P, Trivedi M, Shah P, Singhal A, et al. EFF-1 fusogen promotes phagosome sealing during cell process clearance in Caenorhabditis elegans. Nat Cell Biol. 2018;20(4):393-9.
34. Chiorazzi M, Rui L, Yang Y, Ceribelli M, Tishbi N, Maurer CW, et al. Related F-box proteins control cell death in Caenorhabditis elegans and human lymphoma. Proc Natl Acad Sci U S A. 2013;110(10):3943-8.
35. Jiang HS, Ghose P, Han HF, Wu YZ, Tsai YY, Lin HC, et al. BLMP-1 promotes developmental cell death in C. elegans by timely repression of ced-9 transcription. Development. 2021;148(20).
36. Maurer CW, Chiorazzi M, Shaham S. Timing of the onset of a developmental cell death is controlled by transcriptional induction of the C. elegans ced-3 caspase-encoding gene. Development. 2007;134(7):1357-68.
37. Conradt B, Wu YC, Xue D. Programmed Cell Death During Caenorhabditis elegans Development. Genetics. 2016;203(4):1533-62.
38. Sulston JE, Schierenberg E, White JG, Thomson JN. The embryonic cell lineage of the nematode Caenorhabditis elegans. Dev Biol. 1983;100(1):64-119.
39. Ziegler U, Groscurth P. Morphological features of cell death. News Physiol Sci. 2004;19:124-8.
40. Howell K, Arur S, Schedl T, Sundaram MV. EOR-2 is an obligate binding partner of the BTB-zinc finger protein EOR-1 in Caenorhabditis elegans. Genetics. 2010;184(4):899-913.
41. Niu W, Lu ZJ, Zhong M, Sarov M, Murray JI, Brdlik CM, et al. Diverse transcription factor binding features revealed by genome-wide ChIP-seq in C. elegans. Genome Res. 2011;21(2):245-54.
42. Gerstein MB, Lu ZJ, Van Nostrand EL, Cheng C, Arshinoff BI, Liu T, et al. Integrative analysis of the Caenorhabditis elegans genome by the modENCODE project. Science. 2010;330(6012):1775-87.
43. Parrish J, Li L, Klotz K, Ledwich D, Wang X, Xue D. Mitochondrial endonuclease G is important for apoptosis in C. elegans. Nature. 2001;412(6842):90-4.
44. Ma A, Feng Q, Li P, Yuan L, Xiao H. SCAV-3 affects apoptotic cell degradation in Caenorhabditis elegans. FEBS Open Bio. 2023;13(5):867-80.
45. Wu YC, Stanfield GM, Horvitz HR. NUC-1, a caenorhabditis elegans DNase II homolog, functions in an intermediate step of DNA degradation during apoptosis. Genes Dev. 2000;14(5):536-48.

Time

Rather et. al, FIGURE 1

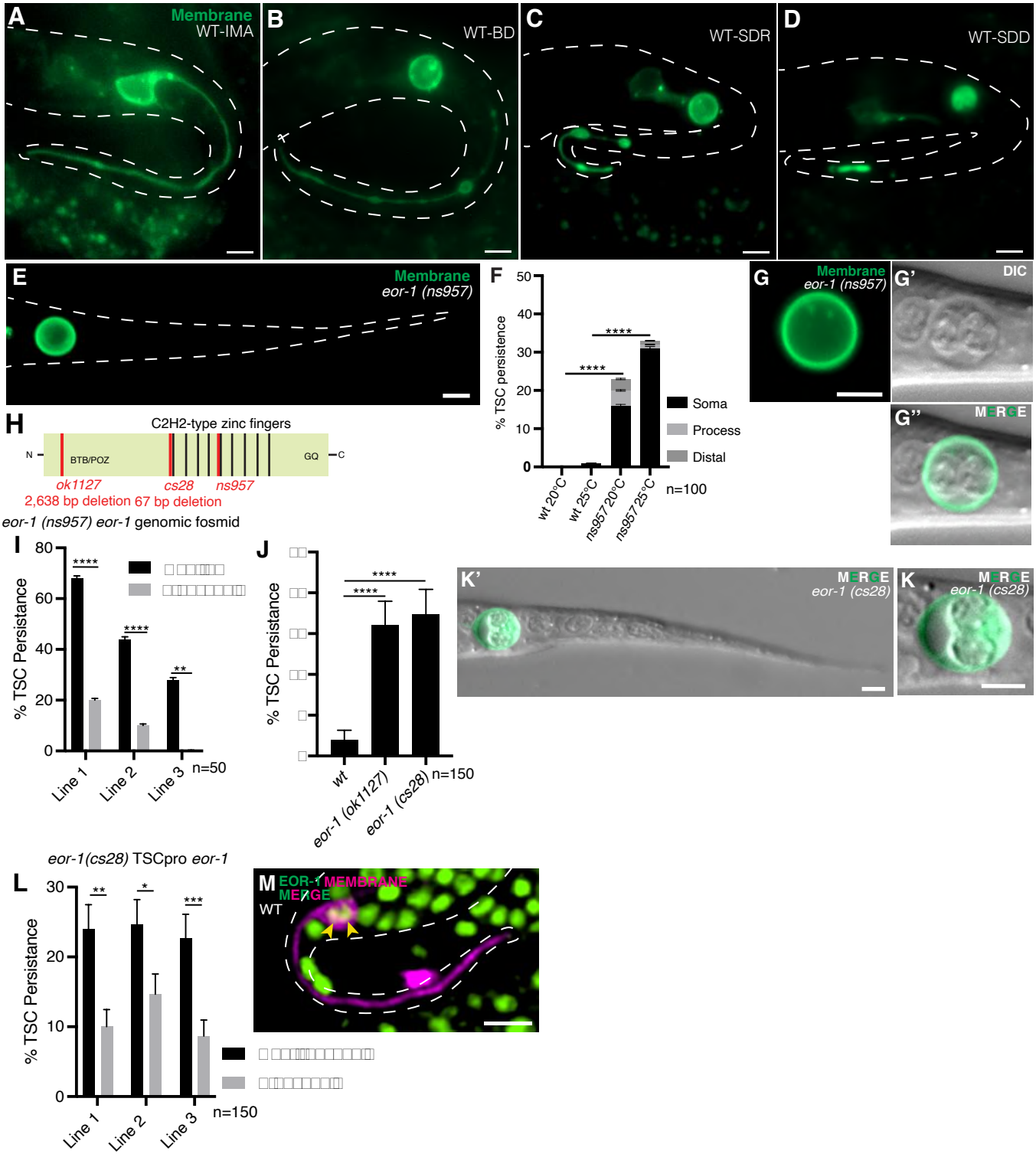

Rather et. al, FIGURE 2

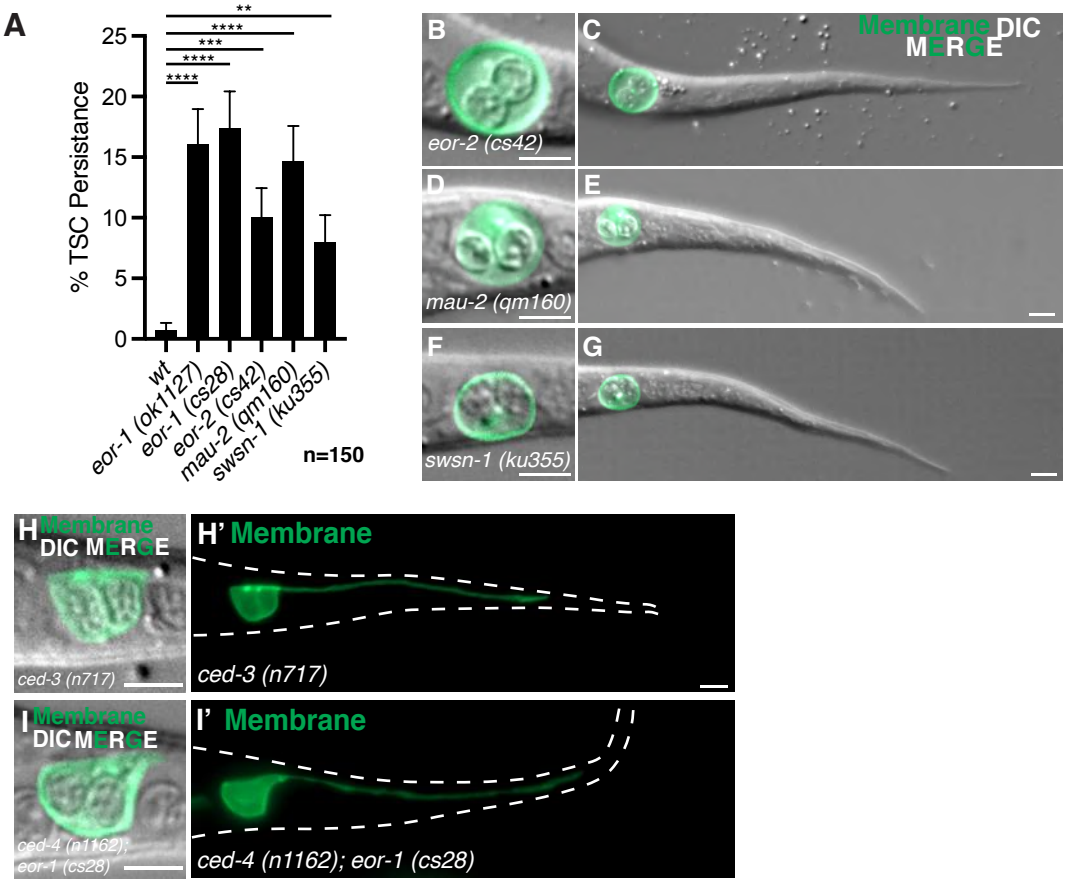

Rather et. al, FIGURE 3

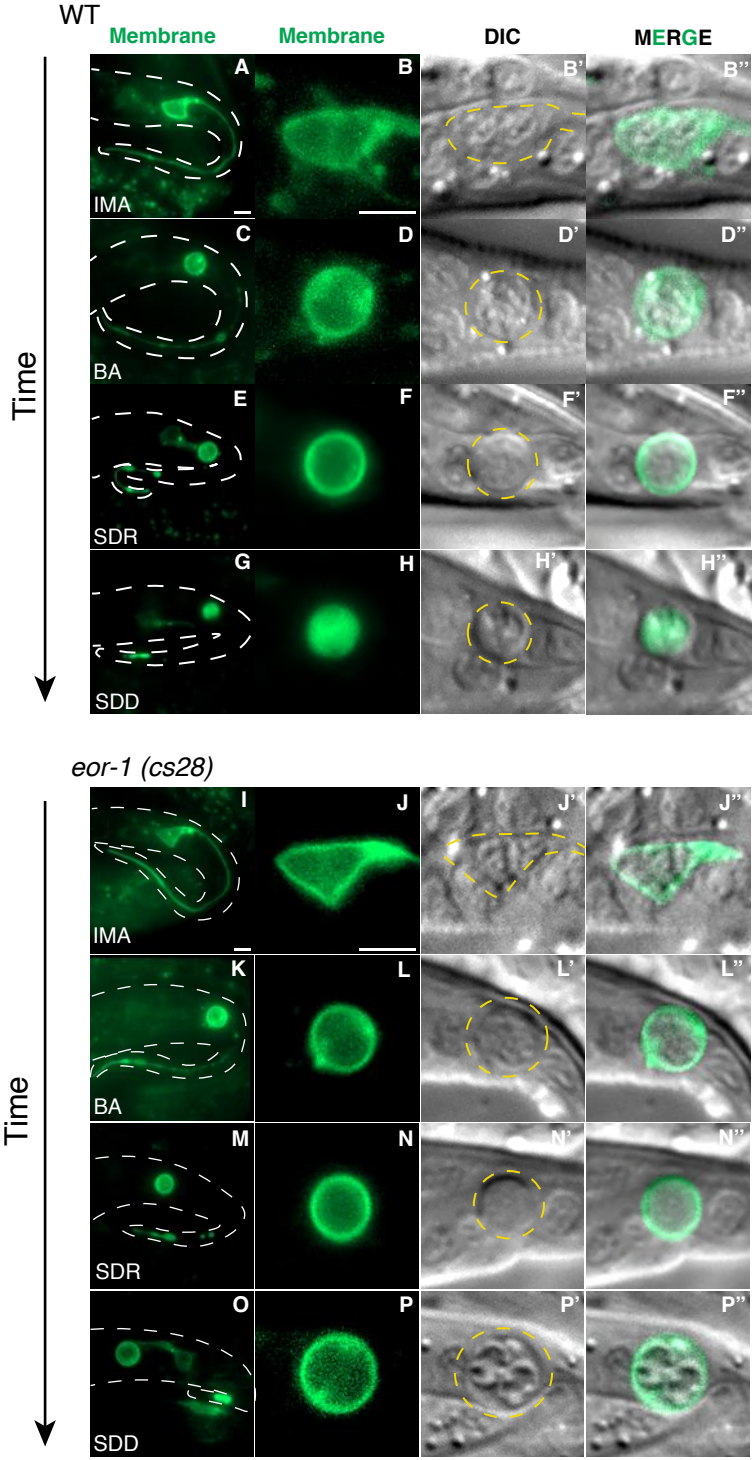

Rather et. al, FIGURE 4

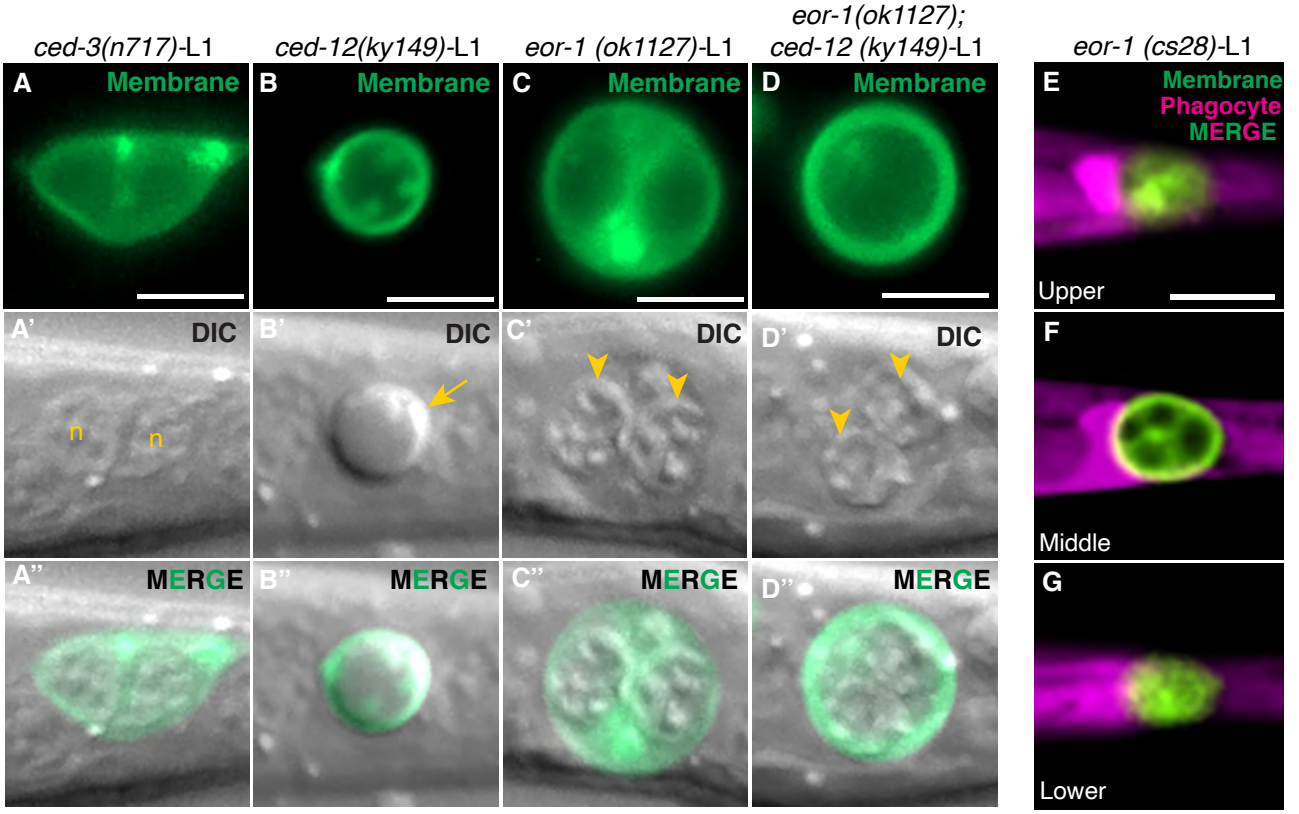

Rather et. al, FIGURE 5

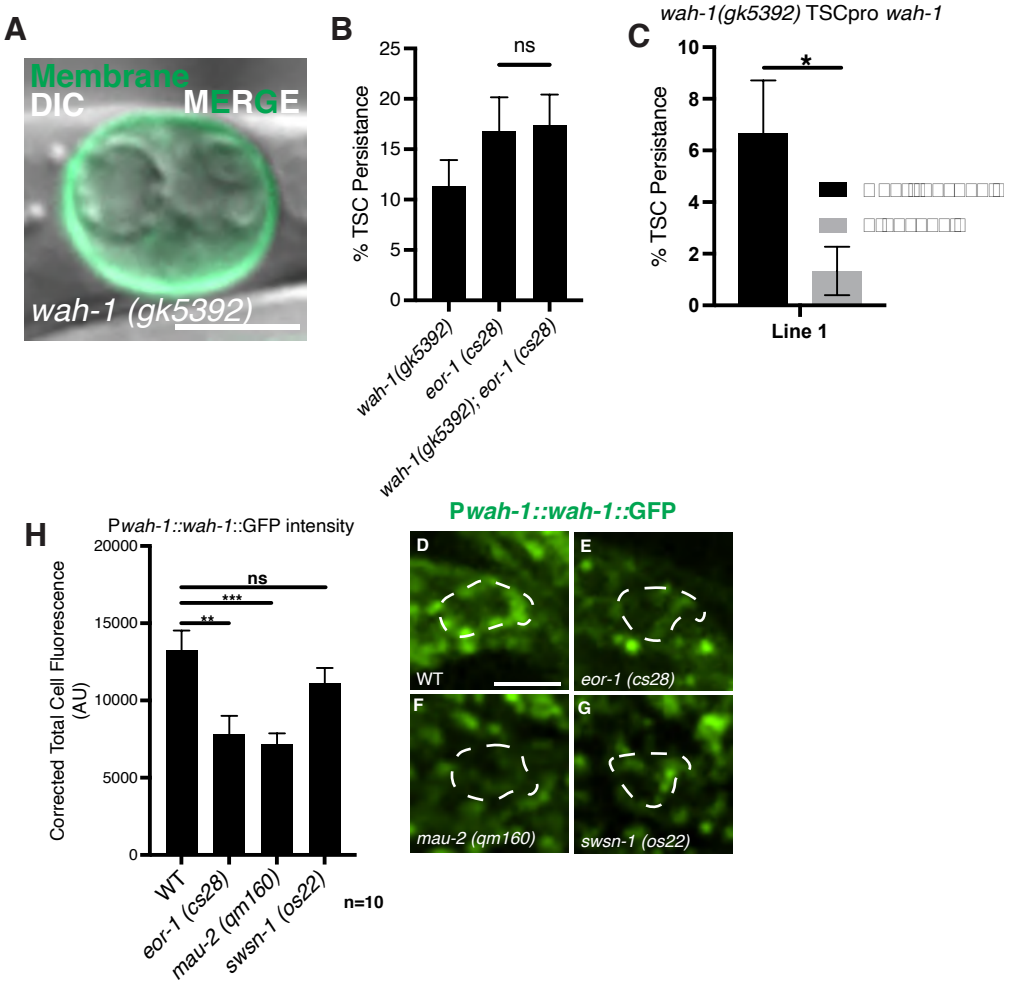

Rather et. al, FIGURE 6

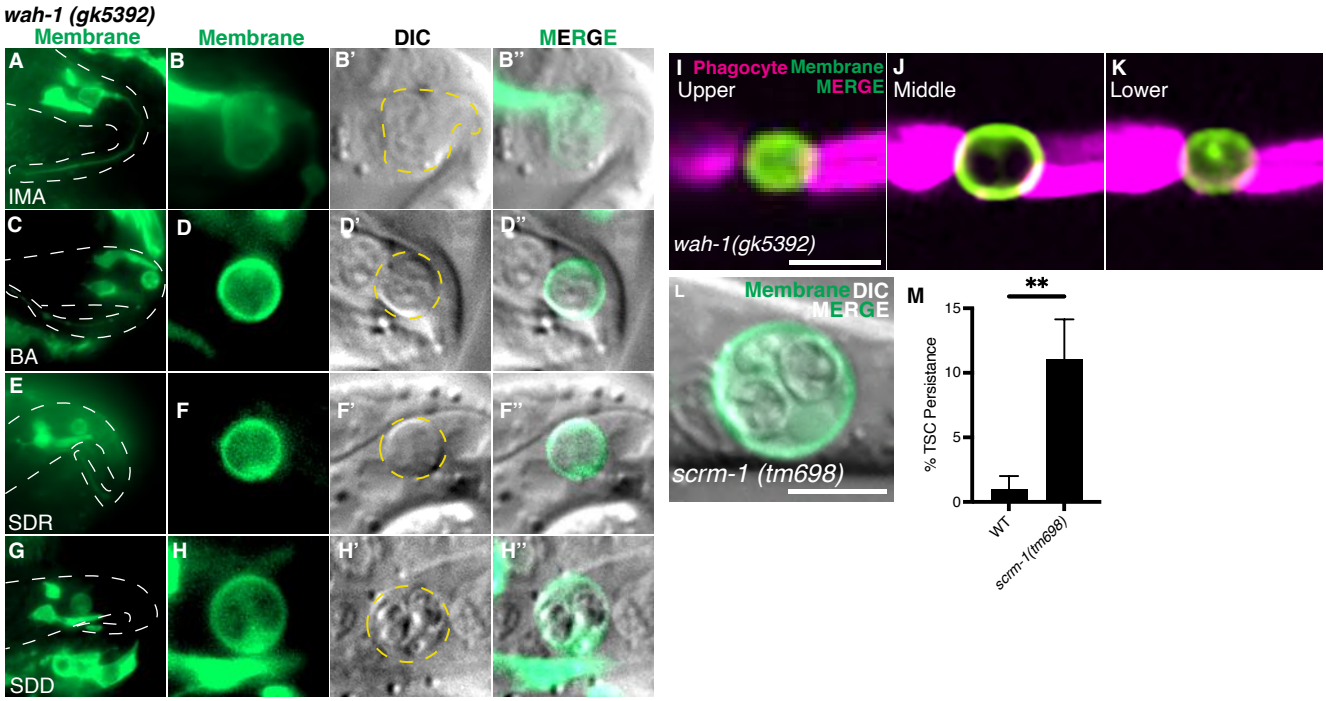

Rather et. al, FIGURE 7

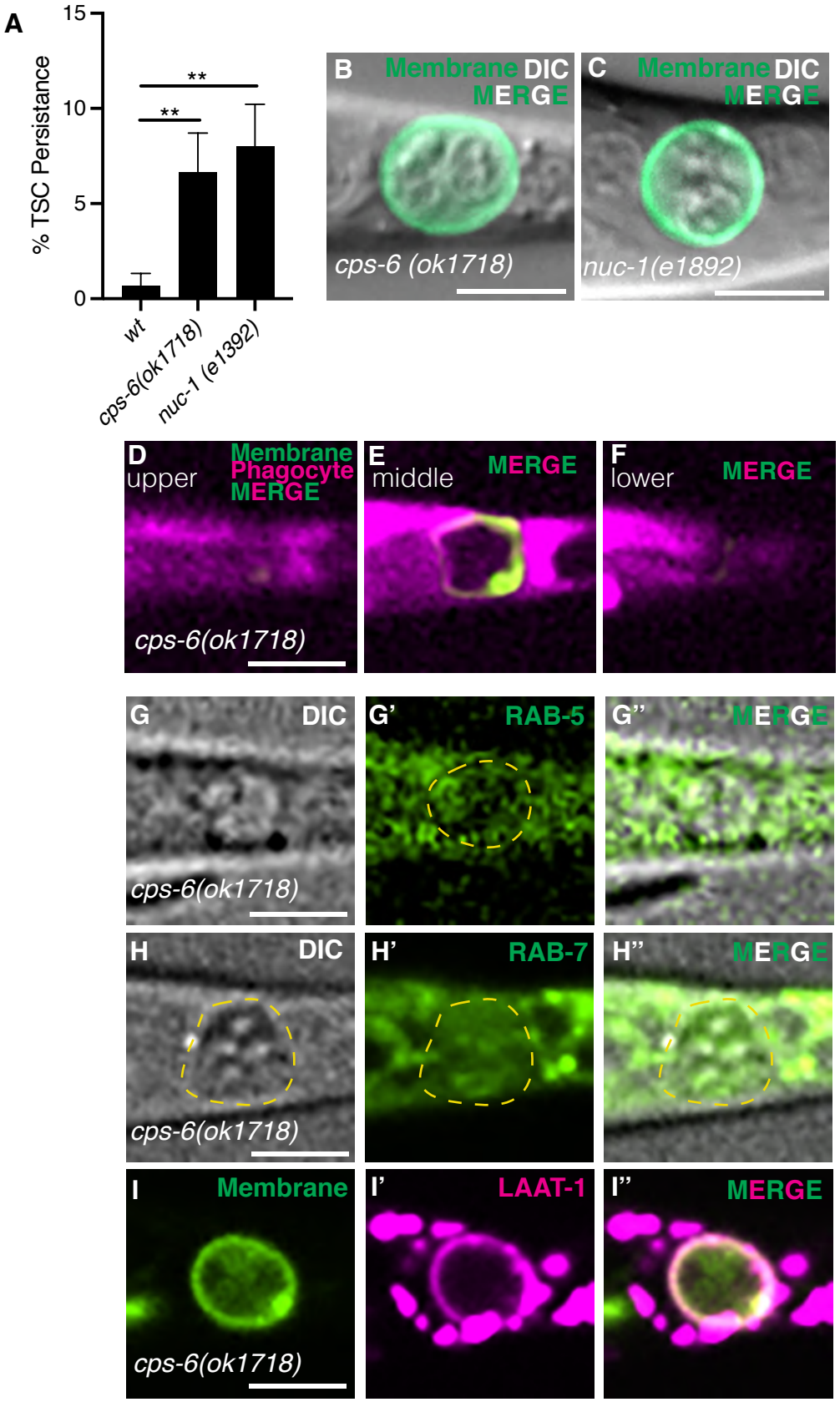

Rather et. al, FIGURE 8

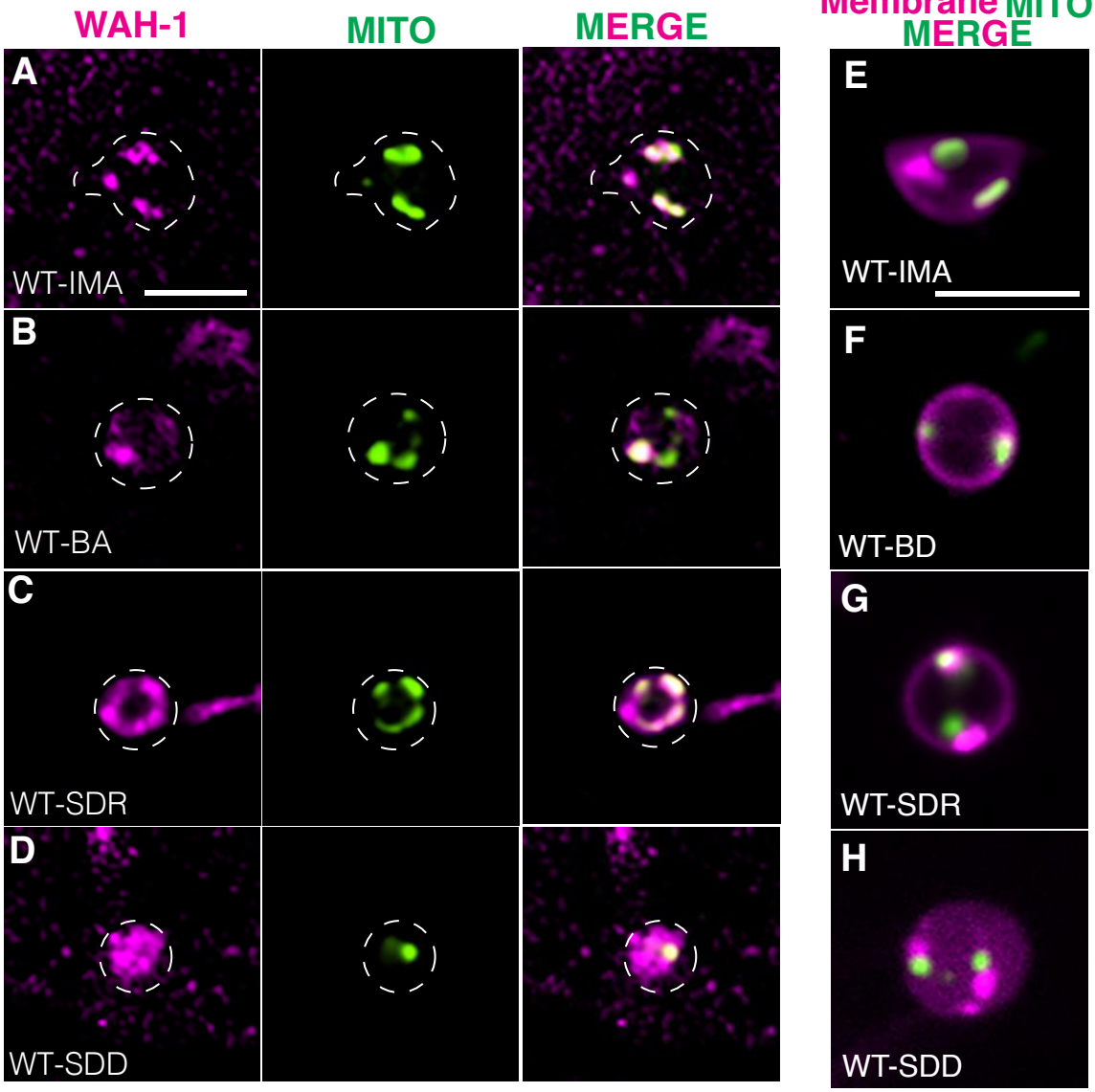

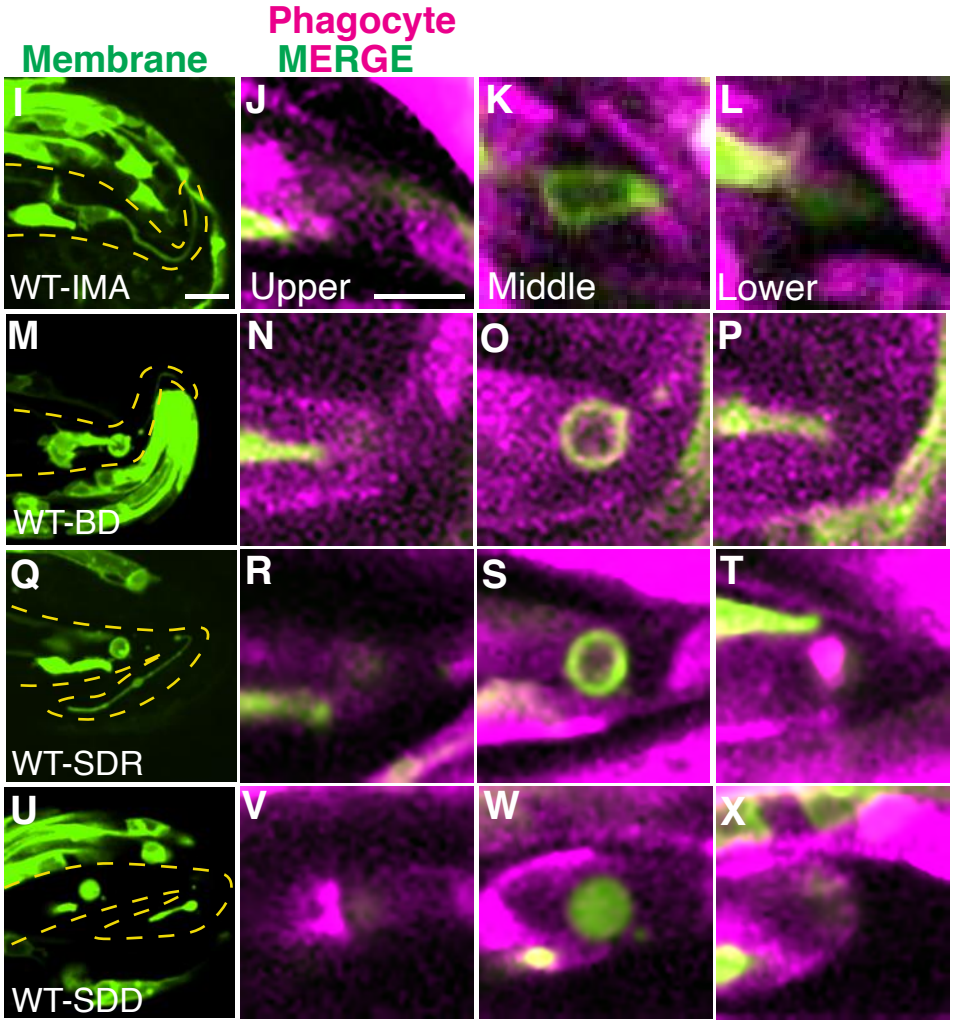
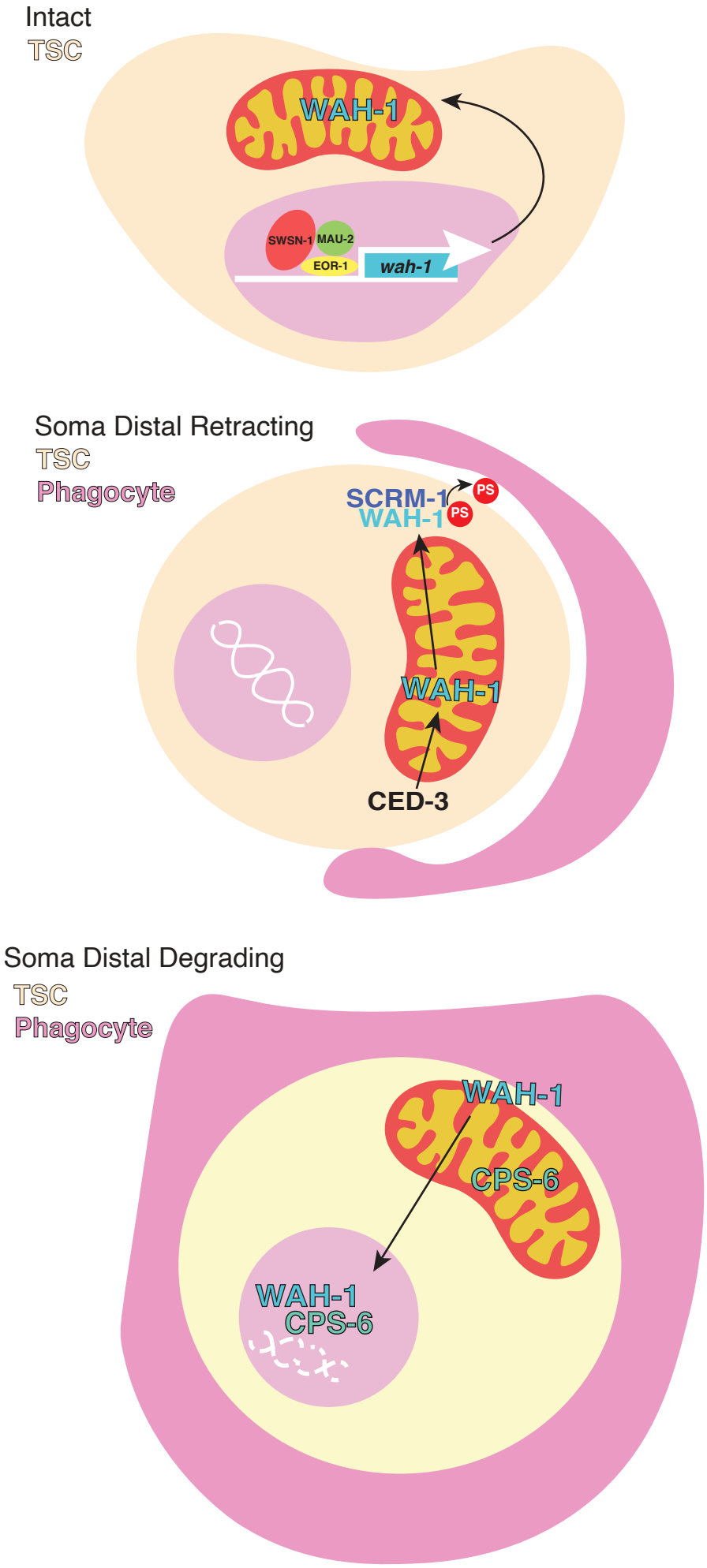
Rather et al Figure 9